Supplementary Materials for

Engineering synthetic morphogen systems that can program multicellular patterning

Satoshi Toda*, Wesley L. McKeithan, Teemu J. Hakkinen, Pilar Lopez, Ophir D. Klein, Wendell A. Lim*

*Corresponding author. Email: wendell.lim@ucsf.edu (W.A.L.); satoshi.toda@staff.kanazawa-u.ac.jp (S.T.)

Published 16 October 2020, *Science* **370**, 327 (2020)
DOI: 10.1126/science.abc0033

This PDF file includes:

Other Supplementary Material for this manuscript includes the following:
(available at science.sciencemag.org/content/370/6514/327/suppl/DC1)

MDAR Reproducibility Checklist (.pdf)
Movies S1 and S2 (.mp4)

Materials and Methods

synNotch Receptor and Ligand Construct Design

synNotch receptors were built by fusing anti-GFP nanobody LaG17, LaG16, LaG9 or anti-mCherry nanobody LaM4 (*9*) to the mouse Notch1 (NM_008714) minimal regulatory region (Ile1427 to Arg1752) and TetR-VP64 (tTA) (*8*). All synNotch receptors contain an N-terminal CD8a signal sequence (MALPVTALLLPLALLLHAARP) for membrane targeting. myc-tag (EQKLISEEDL) for LaG17, LaG16, LaG9 synNotches or FLAG-tag (DYKDDDDK) for LaM4 synNotch to detect their surface expression with anti-myc-Alexa647 antibody (Cell signaling Technology #2233S) and anti-FLAG-Alexa647 antibody (R&D Systems #IC8529R). The receptors were cloned into a modified pHR'SIN:CSW vector containing EF1a promoter. The membrane-tethered GFP (GFPlig, a fusion protein of GFP and PDGFR transmembrane domain) and membrane-tethered mCherry (mCherrylig, a fusion protein of mCherry and PDGFR transmembrane domain) were also cloned into modified pHR'SIN:CSW vector with EF1a or SFFV promoter. All plasmid constructs in this paper were cloned via Infusion cloning (Clontech #ST0345).

Synthetic Morphogen and Anchor Construct Design

To make GFP secreted, we fused Gaussia Luciferase signal sequence (MGVKVLFALICIAVAEA) (*19*) at the N-terminus of GFP. We tandemly fused Gaussia Luciferase signal sequence, mCherry, EAAAK linker (LVGEAAAKEAAAKA) and PNE tag to develop mCherry-PNE morphogen. GFP-fused Shh construct was a gift from Dr. Andrew McMahon (*20*). For the GFP anchor proteins, we tandemly fused CD8a signal sequence, myc tag, anti-GFP nanobody (LaG17, LaG16, LaG9 or LaG2) and the PDGFR transmembrane domain. We also cloned HA-tagged LaG2 anchor protein to establish the hybrid anchor/receiver cell which expresses both myc-tagged LaG17 synNotch and HA-tagged LaG2 anchor. To construct anti-PNE anchor, we tandemly fused CD8a signal sequence, myc or HA tag, anti-PNE scFv C11L34 (*21*) and the PDGFR transmembrane domain. These synthetic morphogens and anchor proteins were cloned into a modified pHR'SIN:CSW vector containing EF1a promoter.

Development of anti-synthetic morphogen inhibitor

To construct expression vectors of soluble anti-GFP nanobody (LaG17, LaG16, LaG9, LaG2 or LaG16LaG2 (LaG16 tandemly fused with LaG2 via 3xGGGGS linker)), we fused Gaussia Luciferase signal sequence and myc tag to the N-terminus of anti-GFP nanobody. We also connected NLS (Nucleus localized Signal)-fused IFP2.0 (*22*) (NLS-IFP) to each soluble LaG construct via P2A ribosomal skipping sequence to monitor their expression. These soluble LaG expression cassettes were cloned into a modified pHR'SIN:CSW vector containing EF1a promoter. We lentivirally transduced these vectors to L929 cells and sorted IFP-positive populations. Then we co-cultured $1x10^4$ GFPlig-expressing cells, $1x10^4$ LaG17 synNotch-expressing receiver cells and $1x10^4$ IFP-positive cells which express soluble LaG protein and analyzed which soluble LaG can efficiently inhibit anti-GFP synNotch activation by GFPlig with flow cytometry LSRII (BD Biosciences). As soluble LaG16LaG2, a fusion protein of two anti-GFP nanobodies, inhibited LaG17 synNotch activation most efficiently, we designed anti-mCherry-PNE inhibitor by fusing anti-PNE scFv and anti-mCherry nanobody. We tandemly fused Gaussia Luciferase signal sequence, myc tag, anti-PNE scFv 52SR4 (higher affinity to PNE tag than C11L34 (*23*)), 3xGGGGS linker and LaM4. We co-cultured $5x10^3$ mCherry-PNE-secreting cells, $5x10^3$ anti-PNE anchor-expressing cells, $5x10^3$ anti-mCherry synNotch-expressing receiver

cells and $5x10^3$ anti-mCherry-PNE-inhibitor-expressing cells to analyze the inhibitory effect on synNotch activation by mCherry-PNE morphogen with flow cytometry.

synNotch Response Element Construct design

The pHR'SIN:CSW vector was also engineered to construct the synNotch response element plasmids. Seven copies of the tetracycline responsive element (TRE, TCCCTATCAGTGATAGAGA) were cloned at 5' to a minimal CMV promoter. In the downstream of this TRE promoter, we cloned following synNotch response elements;
TRE-->mCherry_PGK-->BFP: TRE promoter driving mCherry reporter with PGK promoter driving BFP as an integration marker. (used in LaG17 synNotch receiver cells inducing mCherry reporter)
TRE-->sGFP-P2A-mCherry: TRE promoter driving soluble GFP and mCherry reporter via P2A ribosomal skipping sequence. (used in positive feedback circuit in Fig.3, Fig.4, Fig.S7 Fig.S8)
TRE-->sLaG16LaG2-P2A-NLS-IFP2.0: TRE promoter driving soluble LaG16LaG2 anti-GFP inhibitor and NLS-IFP reporter via P2A. (used in negative feedback circuit in Fig.3, Fig.S7)
TRE-->sGFP-P2A-BFP: TRE promoter driving soluble GFP and BFP reporter via P2A. (used in Fig.2, Fig.4, Fig.S3, Fig.S6, Fig.S8)
TRE-->sGFP-P2A- NLSIFP2.0: TRE promoter driving soluble GFP and NLS-IFP reporter via P2A. (Fig.4, Fig.S8)
TRE-->NLS-IFP2.0_PGK-->puro: TRE promoter driving NLS-IFP reporter with PGK promoter driving puro resistance gene for drug selection. (Fig.S3)

Cell Lines

The mouse fibroblast cell line L929 (ATCC# CCL-1) was cultured in DMEM (Gibco) containing 10% fetal bovine serum (University of California, San Francisco [UCSF] Cell Culture Facility) with penicillin and streptomycin. The human erythroleukemic cell line K562 (ATCC# CCL-243) was lentivirally transduced to stably express GFPlig or mCherrylig to stimulate anti-GFP or anti-mCherry synNotches (Fig.S7, Fig.S8). These K562 cell lines were sorted for the ligand expression. All cell cultures were maintained in an incubator at 37 °C with 5% CO_2 and humidity.

Engineering of L929 cells with synNotch circuits

To induce homogeneous cell behaviors with synNotch circuits, we established clonal receiver cell lines expressing synNotch and its response element. To produce the lentivirus, we plated $7x10^5$ Lenti-X-293T cells in 6 well plate and transfected the pHR'SIN:CSW vector containing synNotch expression cassette or synNotch response element with packaging plasmids (pMD2.G and pCMV-dR8.2) using FuGENE HD (Promega #E2311). For lentiviral transduction, $1x10^5$ L929 cells were plated in 12-well plate and incubated with variable amounts of mixed viral supernatant of both synNotch expression cassete and synNotch response element in the presence of 4 μg/ml polybrene. Three days after transduction, cells were split into two wells in 12-well plate. Next day, we added $1x10^6$ K562 cells expressing synNotch ligand into one well. After 24hr co-culture, we analyzed basal/induced expression level of target fluorescence proteins with or without synNotch stimulation by the K562 cells and sorted the cells into 96 well plate at single cell per well via a cell sorter FACS Aria Fusion (BD Biosciences). After cells grew, we screened clones by measuring the basal/induced expression level of target fluorescence proteins with or without stimulation by K562 expressing synNotch ligand and picked up several clones which have low

basal expression but high induction of target genes. We show the basal/induced expression level of reporter genes in receiver cells for positive and negative feedback circuit and two receiver cells for three domain patterns in Fig. S7 and S8.

Gradient formation assay

To create the "pole" and "body" region in a tissue culture plate, we put the 2-well insert-wall (Ibidi #80209) in the center of the well in 24-well plate (Fig.S2A). Then we plated $3x10^4$ GFP-secreting cells in 75ul of media into the left pole regionl and $1.5x10^4$ cells of LaG2 anchor cell and LaG17 synNotch receiver cell (homogeneous mixture of $0.75x10^4$ cells of each cell type) in 75ul of media into the right body region. We also plated $6x10^4$ cells of the anchor and receiver mixture cells in 300ul of media into the outside of the insert-wall as a sink. Then we incubated the plate for 5 hours in the CO_2 incubator to attach the cells on the plate. We gently washed the pole region with 75ul of fresh media twice to remove GFP secreted during 5hr incubation and removed the insert wall with sterile tweezer. We then aspirated the media and added 800ul of media containing 1% agarose (Sigma-Aldrich #A9045-5G) using 5ml serological pipette. The media containing 1% agarose was prepared by mixing the same volume of DMEM containing 20%FBS and PBS containing 2% agarose. We imaged the plates with either IncuCyte (Sartorius), IN Cell Analyzer 6000 (GE Healthcare) or Opera Phenix (Perkin Elmer) for time-lapse imaging. For the mCherry-PNE morphogen studies, we plated mCherry-PNE-secreting cells in the pole region and $1.5x10^4$ cells of mixture of anti-PNE anchor cell and anti-mCherry receiver cell (50:50). In Fig.S3, we fixed the total number of cells at $3x10^4$ in the pole region and changed the ratio of mCherry-PNE-secreting cells and parental L929 to titrate the amount of mCherry-PNE source. In Fig.1D, we plated $3x10^4$ GFPlig-expressing L929 cells in the pole and $1.5x10^4$ LaG17 synNotch receiver cells in the body to show the signaling range of juxtacrine signaling.

To create the double-pole system, we put the 3-well insert-wall (Ibidi #80369) in the center of the well in 12-well plate (Fig.S2B). We plated $3x10^4$ synthetic morphogen-secreting cells in the left pole region, $1.5x10^4$ anchor and receiver mixture cells in the middle body region and $3x10^4$ inhibitor-secreting cells in the right pole region. We fixed the total number of cells at $3x10^4$ in the right pole region and changed the ratio of inhibitor-secreting cells and parental L929 to titrate the amount of inhibitor source. We also plated $1.5x10^5$ of the anchor and receiver mixture cells in 750ul of media into the outside of the insert-wall as a sink. After cells attached to the plate, we cultured cells in 1.2ml of media containing 1% agarose and imaged the plates as described above. See Table S1 for more detailed information about the number of cells in each region in each figure.

Variations of anchor site densities (Fig.2A and Fig.S4)

To establish the cells that expressed high or low levels of LaG2 anchor used in Fig.2A and Fig.S4A, we transduced L929 cells and LaG17 synNotch receiver cells with 400ul or 100ul of lentiviral supernatant of HA-tagged LaG2 anchor expression vector. Then, we stained the cells with anti-HA antibody-Alexa647 (Cell signaling Technology #3444S) and sorted high-expression population infected with 400ul viral sup (MFI of Alexa647: $>2x10^3$) and low-expression population infected with 100ul viral sup (MFI of Alexa647: $5x10^2$ to $2x10^3$). To confirm the LaG2 anchor expression level, we plated $4x10^4$ cells of the sorted cells in 96well plate and next day stained them with anti-HA-Alexa647 to analyze by flow cytometry (Fig.S4). We finally established cells expressing high or low level of LaG2 anchor (high or low anchor cells) and LaG17 synNotch receiver cells expressing high or low level of LaG2 anchor (high or low hybrid receiver/anchor cells). In Fig.S4, we plated $3x10^4$ GFP-secreting cells in the pole region and

$1.5x10^4$ cells of high or low anchor cells in the body region (100% high or low anchor cells). We also plated $1.5x10^4$ mixture of high or low anchor cells and parental L929 cells to dilute the anchor density (50% high or low anchor cells). We imaged the GFP gradient in the body region using In Cell Analyzer 6000 at 24hr and quantified GFP intensity in a rectangular ROI with ImageJ. In Fig.2A, we plated $3x10^4$ GFP-secreting cells in the pole region and $1.5x10^4$ cells of high or low hybrid receiver/anchor cells (100% HIGH or LOW anchor cells). We also plated $1.5x10^4$ mixture of high or low anchor cells and LaG17 synNotch receiver cells (50% HIGH or LOW anchor cells). We imaged the mCherry reporter output with Incucyte for 5 days and quantified mCherry intensity in a rectangular ROI with ImageJ.

Engineering morphogen cascade for three-domain formation (Fig.4C-D and Fig.S8)

$1.5x10^4$ mixture cells of two types of receiver cells, receiver A and B, (50:50) were plated in the body region. Receiver A cells express anti-mCherry synNotch to recognize mCherryPNE morphogen and induce BFP reporter expression and GFP secretion. Receiver B cells express anti-GFP LaG17 synNotch to detect GFP morphogen and induce IFP reporter and GFP secretion as a positive feedback. Receiver A cells also express LaG2 anchor to serve as anchor cells for Receiver B, while Receiver B cells express anti-PNE anchor as an anchor for Receiver A.

Receiver A: anti-mCherry synNotch → BFP reporter + GFP secretion ; anti-GFP (LaG2) anchor
Receiver B: anti-GFP (LaG17) synNotch → IFP reporter + GFP secretion ; anti-PNE anchor

In Fig.4D, $0.3x10^4$ mCherryPNE-secreting cells and $2.7x10^4$ L929 cells were plated in the left pole and $0.3x10^4$ mCherryPNE inhibitor-secreting cells and $2.7x10^4$ L929 cells were plated in the right pole. In Movie S2, $0.6x10^4$ mCherryPNE-secreting cells and $2.4x10^4$ L929 cells were plated in the left pole and $0.6x10^4$ mCherryPNE inhibitor-secreting cells and $2.4x10^4$ L929 cells were plated in the right pole. $1.5x10^5$ mixture of anti-PNE anchor cells and L929 cells (50:50) were plated outside of poles as a sink.

Sensing soluble GFP with Primary Human T cells (Fig.S10)

Blood was obtained from Blood Centers of the Pacific (San Francisco, CA) as approved by the University Institutional Review Board. Primary CD4+ and CD8+ T cells were isolated from anonymous donor blood after apheresis by negative selection (STEMCELL Technologies #15062 and 15023). T cells were cultured in human T cell medium (hTCM) consisting of X-VIVO 15 (Lonza #04-418Q), 5% Human AB serum and 10 mM neutralized N-acetyl L-Cysteine (Sigma-Aldrich #A9165) supplemented with 30 units/mL IL-2 (NCI BRB Preclinical Repository). Production of lentivirus for transduction was conducted as above (see Engineering of L929 cells with synNotch circuits). Primary T cells were thawed (Day 0) and after 24 hours (Day 1), were stimulated with Dynabeads Human T-Activator CD3/CD28 (Thermo Scientific #11131D) at a 1:3 cell:bead ratio. On Day 2, viral supernatant was collected and mixed with the T cells for 24 hours. The following day (day 4), the viral supernatant was removed and was replaced with fresh hTCM. On day 5, the Dynabeads were removed and the T cells were cultured for 2 more days prior to cell sorting. On day 7, surface expression of both synNotch receptor and Anchor proteins was detected using anti-myc-Alexa647 antibody (Cell signaling Technology #2233S) and cells expressing each construct were subsequently sorted using a FACS Aria Fusion (BD Biosciences). The media was changed every other day for 1 week with fresh hTCM until dose response experiments.

On day 14, T cells expressing anti-GFP synNotch (LaG17 synNotch) and T cells expressing the anti-GFP Anchor (LaG2) were mixed at a 1:1 ratio in a 96 well round bottom plate (100,000 cells total). A 10-fold dilution of purified GFP was subsequently added to each well with the highest concentration of 1 μM. The cells were incubated for 24 hours before analysis by flow cytometry with an LSRII (BS Biosciences). These experiments were conducted in triplicate.

Microscopy and image analysis

Images and movies of mCherry and Phase channels were taken by IncuCyte in a 37°C 5% CO_2 incubator. We run a whole-well imaging with 4x objective every 2 hrs. The raw images were exported with Zoom software and analyzed with ImageJ. We put the rectangle shape of ROI around the center of body region and quantified GFP and mCherry fluorescence intensity. We also quantified the area of mCherry-positive region over a threshold of 25 on mCherry intensity. The movies were exported with fixed range on mCherry channel by the Zoom software.

When receiver cells induce BFP, we used IN Cell Analyzer 6000 to take images of BFP, GFP, mCherry and Phase channels in the body region with non-confocal mode using 10x objective. To quantify the fluorescence intensity, we stitched 6 images around the center of body region to cover the left to right edge of the body region. We then quantified fluorescence intensity with ImageJ.

For the quantification of reporter fluorescence intensity in each experiment, ImageJ macro was used to apply the same ROI and conditions of contrast and brightness to each time-point of time-lapse images. We modified the positions of ROI to be fit to the body position in each sample, which depends on the insert-wall position, and applied the same range of contrast and brightness to each sample to output images. We included some area outside the body region in each ROI and subtracted the minimum value of fluorescence intensity in the ROI as a background. Since stitching the images taken by IN Cell Analyzer 6000 caused a periodic pattern artifact, we took images of the "blank" body region containing only parental L929 as a background and subtracted the fluorescence profile of the blank well from each sample.

To take a movie of three domain formation in Fig.4C, we used Perkin Elmer Opera Phenix automated confocal microscope. Images of BFP, GFP, mCherry and Brightfield were acquired every 2 hours at 37°C and 5% CO_2 using a 10x long working distance air objective (NA = 0.3).

To calculate the signaling range (EC50, $r_{1/2}$) of gradient reporter expression, we smoothened the reporter fluorescence intensity recorded by incucyte in the ROI by taking averages of fluorescence intensity on continuous 9 pixels every 9 pixels (In the case of images recorded by IN Cell Analyzer 6000, we smoothened them every 17 pixels). Then we measured the position of the highest fluorescence intensity (peak position) and the first position where the fluorescence intensity gets below the half value of the highest fluorescence intensity (half-peak position). In some cases, the fluorescence intensity around the half-peak position fluctuated. This case, we picked up the first position where the fluorescence intensity is below the half value and the final position where the fluorescence intensity is above the half value, and then took an average of them as a half-peak position. The signaling range was calculated as a balance of the peak position to the half-peak position.

Computational model

We developed a simple computational model as a tool to identify trends of how key variables cause relative changes in the system behavior. As the physical values of almost all the model parameters, with the exception of dissociation constants K_d, are unknown in the present system, we have deliberately been relatively cautious and attempted to find a minimal system that

can qualitatively account for the basic results of anchor binding and inhibitory action obtained in the experiments. The model describes the time-evolution of the relative distributions (concentrations) of a diffusing free morphogen (i.e., GFP or mCherry-PNE), its inhibitor when applicable, and a non-diffusing secondary signal following the trapping of the free morphogen by anchors. For simplicity, we have implemented the model in one spatial dimension, where the model domain should be understood as representing a thin slice of the experimental setting running from a secreting pole to the opposing pole, approximately at the center and away from the borders. The domain is divided into three parts consisting of a central body and secreting poles for the morphogen and the inhibitor at the oppose ends of the domain. Within the body, denoted by $[B_0, B_1] \subset [P_0, P_1]$, where P_0, P_1 are the pole ends, the model dynamics are:

$$\text{Free morphogen}: \quad \frac{\partial M}{\partial t} = \underbrace{D\nabla^2 M}_{\text{Diffusion}} - \underbrace{k^i_{on} k_\rho M I + k^i_{off} \hat{I}}_{\text{Inhibitor binding}} - \underbrace{k^a_{on} k_\rho M(1-\hat{M}) + k^a_{off}\hat{M}}_{\text{Anchor binding}} - \underbrace{k_{deg} M}_{\text{Degradation}}$$

$$\text{Free inhibitor}: \quad \frac{\partial I}{\partial t} = D\nabla^2 I - k^i_{on} k_\rho M I + k^i_{off}\hat{I} - k_{deg} I$$

$$\text{Trapped morphogen}: \quad \frac{\partial \hat{M}}{\partial t} = k^a_{on} k_\rho M(1-\hat{M}) - k^a_{off}\hat{M} - k_{deg}\hat{M}$$

$$\text{Bound inhibitor}: \quad \frac{\partial \hat{I}}{\partial t} = k^i_{on} k_\rho M I - k^i_{off}\hat{I} - k_{deg}\hat{I}$$

where *D* denotes the diffusion rate (morphogens trapped to anchors or the inhibitor do not diffuse), $\boldsymbol{k_{on}}$ and $\boldsymbol{k_{off}}$ the binding and unbinding rates with superscripts indicating the molecule, $\boldsymbol{k_p}$ the effective concentrations and k_{deg} degradation rate. To model the secretion of the free morphogen and its inhibitor at the opposing poles, constant sources are set at the respective ends of the computational domain, in $[P_0, B_0)$ for the morphogen and in $(B_1, P_1]$ for the inhibitor. Within these secreting bands the binding dynamics are suspended, and only the morphogen degradation and diffusion are present in addition to a source:

$$\frac{\partial C}{\partial t} = D\nabla^2 C + k^c_{src} - k_{deg} C$$

where *C* is either the free morphogen or the inhibitor concentration, depending on the pole, and k_{src} the corresponding pole source constant (production rate). We consider the decay term to incorporate both the dedicated sink and the general degradation. The boundary conditions at P_0, P_1 are set as zero Neumann (no flux). All concentrations are initialized as zeros. The concentration of the trapped morphogen $\boldsymbol{\hat{M}}$ is the main readout of the model: It is understood as a proxy of the transcriptional responses of the receptor cells.

In our simulations, we used arbitrary values for most of the parameters, but used relative changes that reflect the relative perturbations we made in our experiments when possible (e.g. we used relative anchor densities of 2, 1 and 1/2, reflecting the range of perturbations used in the experiments shown in Fig. 2A). With the exception of Figs. S5A and S5B, as outlined below, common parameter values were used for all the free model parameters (those with unknown values) across the simulations. The use of common values for the parameters is not meant to

indicate our understanding of what the actual physical values of those parameters are; for example, there is no reason to assume that the diffusion rate is exactly the same for all GFP, mCherry-PNE and their inhibitors. A more accurate model and analysis of the physically realistic parameter values will be left to a future work.

For simplicity and due to largely undetermined nature of the system, we considered all the parameters as dimensionless quantities. The base parameter values used in all simulations unless otherwise stated are: D = 0.01, $k_\rho^a = k_\rho^i$ = 1e-07, k_{deg}= 0.02, k_{src}^m = 1.0. A fixed off-rate was assumed for all inhibitors and anchors $k_{off}^i = k_{off}^a$ = 2e-4, and the corresponding on-rates where directly computed from the known dissociation constants K_d as $k_{on} = k_{off} / K_d$. The variations of parameter values in each figure were as follows:

Fig. S5A (left): With morphogen production k_{src}^m = 0.1, the anchor on-rate is varied with k_{on}^a from the known K_d values of 50e-9, 3.5e-9, 0.7e-9 (units M) for LaG17, LaG16 and LaG9, respectively. No inhibitor.

Fig. S5A (right): Anchor on-rate k_{on}^a was modulated with multipliers of 1, 10, 100, 400 around the base value set from K_d = 16e-9 (LaG2). No inhibitor.

Fig. S5B (left): With k_{on}^a set from K_d = 16e-09 (LaG2), and with morphogen production k_{src}^m = 0.1, degradation k_{deg} = 0.01, modulating anchor density with k_ρ^a = 2e-05, 1e-05, 0.5e-05. No inhibitor.

Fig. S5B (right): With k_{on}^a set from K_d = 40e-12 (mCherry-PNE), modulating anchor density with k_ρ^a = 0.25e-07, 0.5e-07, 1e-07. No inhibitor.

Fig. S5C (left): With k_{on}^a set from K_d = 16e-09 (LaG2) and k_{on}^i from K_d = 0.036e-09 (LaG16LaG2), modulating inhibitor production k_{src}^i = 0.0, 0.25, 0.5.

Fig. S5C (right): With k_{on}^a from K_d = 40e-12 (mCherry-PNE) and k_{on}^i from K_d = 5e-12 (52SR4), modulating inhibitor production with k_{src}^i = 0.0, 0.5, 1.5, 5.0 (included in S5C only).

An alternative simulation of Fig. S5A (not shown) was performed, where the actual on-off rates k_{on}^a, k_{off}^a known for the three LaGs were used. With these values the same relative trends as shown in Fig. S5A were obtained, but only after scaling diffusion, degradation, morphogen source and receptor densities down to approximately 1% of their current values. Such additional constraining of the system might give clues of the physically realistic parameter values.

One complication in our simulation work arose from the fact that affinities indicated by the dissociation constants K_d alone didn't explain the effective binding rates across all cases. This was in particular the case with LaG2 as an anchor molecule compared to other LaGs as anchors, as shown in Fig. S1A: While the relative trapping rates as represented by the GFP intensity could be directly predicted (Fig. S5A, left) from the known dissociation constants for the three LaGs belonging to the same epitome group I (LaG17, LaG16, LaG9), LaG2 belonging to a different epitome group II stood out from the rest. While a closer look at the actual on-off rates (since $K_d = k_{off} / k_{on}$), known for the LaGs in epitome group I suggested that a different scaling of the free model parameters (diffusion, degradation etc.) might be needed, this wasn't sufficient to explain

the effective trapping rate of LaG2. This suggested that an accurate modeling of the trapping kinetics across different epitome groups would require considering additional mechanisms or factors beyond the simple affinity rates and molecular densities. Because of this, and also because the present system is largely undetermined when it comes to most model parameters (diffusion, degradation etc.), the presented simulations should be taken more as a support of the interpretations made from the data, rather than as an attempt to prove them.

All simulations represent the steady state of the system. The model may be considered robust in that small relative changes in the parameter values do not change the general trends or affect the conclusions. The equations were solved using the explicit Euler method in MATLAB, for which the domain in [0, 1] was divided into 80 nodes, with the first and the last nodes dedicated to the poles and the remaining 78 nodes for the body. Steady states were obtained in each case by computing until time $T = 2$ with time step $\Delta t = 0.002$. The results were verified to be insensitive to the increase of both the temporal and spatial resolution. While modulating the relative width of the poles when other parameters were fixed affected the model behavior, the overall conclusions were not affected, and the differences due to varying pole widths were effectively cancelled by a different scaling of the free parameters (production rates most importantly) whose absolute values were not fixed in the first place. Similarly, we investigated different implementations for the sink, but we found its effect to be minor in the presence of general degradation, hence for simplicity we have included only a single degradation term encompassing both the sink and the actual degradation.

Supplementary text

Development of mCherry-PNE synthetic morphogen

We tested another bivalently recognized protein by designing a fusion protein of mCherry with a PNE peptide tag as a second synthetic morphogen (mCherry-PNE). To detect this, we used an anti-mCherry nanobody (LaM4) and an anti-PNE scFv (C11L34) as receptor and anchor interaction domains, respectively (**Fig.S3**) (*9,23*). We setup the similar in vitro gradient assay for mCherry-PNE morphogen: "pole" region composed of mCherry-PNE-secreting cells and "body" region anti-PNE anchor cells and anti-PNE synNotch receiver cells. We found that mCherry-PNE also formed a gradient of reporter gene expression within the body region (**Fig.S3**). Thus, multiple arbitrary proteins (with two binding sites) can be turned into morphogens (**Fig.1B**), suggesting that many more potential synthetic morphogen systems could be developed.

Testing variations of anti-GFP nanobodies for the anchor protein

We tested mutated variants of anti-GFP nanobodies, LaG9, LaG16, and LaG17 for the anchor protein, that bind the same epitope on GFP with differing affinities (**Fig.S1A**)(*9*). GFP-secreting cells and anchor-expressing cells were plated in the pole and body region respectively. We found that the high-affinity LaG16 anchor (K_d = 0.7nM) tethered more GFP than lower-affinity LaG9 anchor (K_d = 3.5nM). Almost no GFP was tethered by the lowest affinity LaG17 anchor (K_d = 50nM). LaG2 (K_d = 16nM), which binds a distinct epitope, showed the highest capacity to tether GFP, suggesting that both affinity and details of the binding site are important (**Fig.S1A**). The GFP fluorescence intensity can be potentially changed by binding to nanobodies, which could influence the quantification of GFP gradient. In the SPR measurement condition, GFP fluorescence intensity is slightly increased by binding to LaG nanobodies (*9*).

Developmet of an anti-synthetic morphogen inhibitor

To develop an anti-synthetic morphogen inhibitor, we tested which anti-GFP nanobodies in soluble form could inhibit GFP synNotch activation. We cocultured GFP-secreting cells, LaG2 anchor cells, LaG17 synNotch receiver cells and inhibitor cells that secrete soluble anti-GFP nanobodies. We found that only a tandem anti-GFP nanobody (fusion of LaG16-LaG2) could efficiently inhibit LaG17 synNotch activation (**Fig.S6A**). We also developed a comparable soluble inhibitor for the mCherry-PNE morphogen (fusion of anti-mCherry nanobody and anti-PNE scFv) (**Fig.S6B**).

Discussion on the difference of inhibitor effects for GFP and mCherry-PNE morphogens

While the GFP inhibitor secreted from the opposing pole reduced amplitude of the activation gradient generated by the GFP morphogen (**Fig.S6C**), the mCherry-PNE inhibitor reduced the signaling range of the activation gradient generated by mCherry-PNE morphogen with smaller effects on amplitude (**Fig.2B**). This difference in how the inhibitor pole dampens morphogen signaling may be caused by the >100-fold difference in affinities of the anchor-morphogen interactions (mCherry-PNE K_d = 40 pM; GFP LaG2 K_d =16 nM). Under these conditions, the computational model predicted that mCherry-PNE anchors are more likely approaching saturation close to the morphogen source, leading to reduced inhibitor sensitivity near the morphogen pole (**Fig.S5A**). The trends predicted by computational model with inhibitor-secreting pole show two types of behaviors with different affinity range of morphogen and

inhibitor: the reduction of amplitude in an affinity range of GFP morphogen/inhibitor system and the reduction of signaling range with higher-affinity mCherry-PNE morphogen/inhibitor system, which is consistent with our observations in **Fig.2B** and **Fig.S5C**.

Further discussion on synthetic morphogen system

The difference between natural morphogens and our synthetic morphogens is that the synthetic morphogens need to be tethered by anchor proteins to activate their receptors (synNotch receptor), while natural morphogens can directly activate their receptors by themselves. This point is a limitation of our synthetic morphogen system, but most natural morphogens also associate with additional anchoring factors such as glypican, ECM and cell membrane to regulate signaling range and prevent leakage into circulation. Indeed, we found GFP fused with Shh (*20*) could activate anti-GFP synNotch receptors directly, without the need for additional anchoring interactions (**Fig.S10**), implying that the Shh morphogen is tethered and localized on cell surface. Therefore, the modularity of our synthetic morphogen systems makes them a highly flexible toolkit with which to systematically explore and test design principles of morphogen gradient shaping and multicellular patterning (**Fig. S9B**). We have only built a small fraction of possible synthetic patterning circuits, and there are many other mechanisms for regulating morphogen signaling that we have not explored, including ultrasensitive intracellular transcriptional responses (*24*,*25*) and degradation/shuttling of morphogens (*26*).

Fig. S1. Testing diffusible GFP synNotch sensing system

A. Analyzing different GFP nanobodies as Anchor molecules

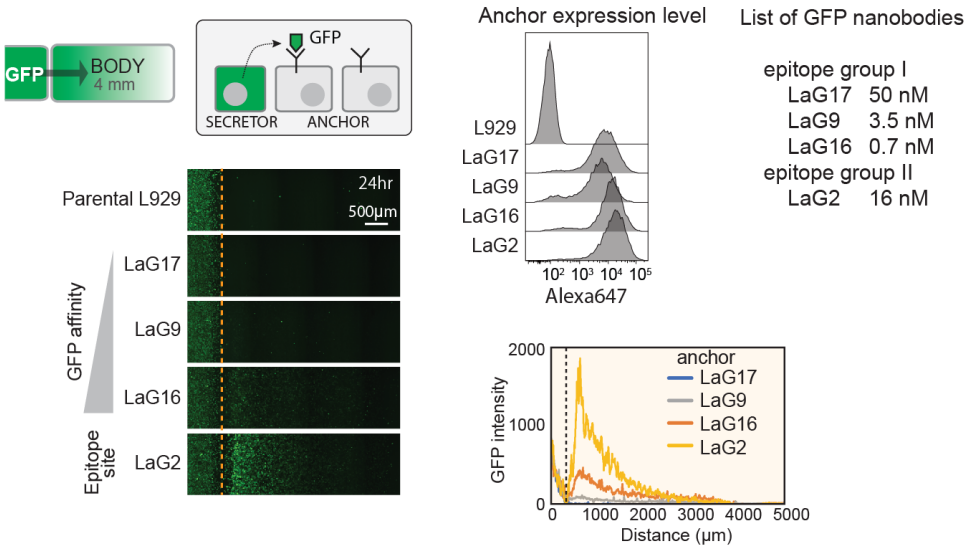

B. SynNotch activation with purified GFP and Anchor cells

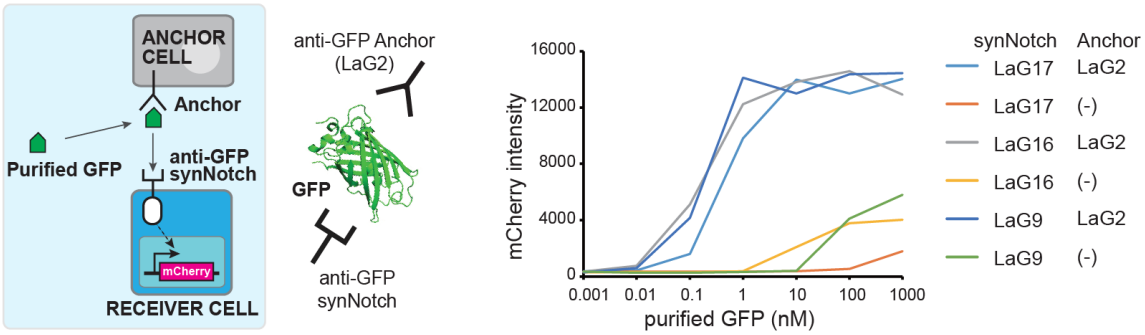

C. Dose-dependent synNotch activation by GFP-secreting cells with Anchor cells

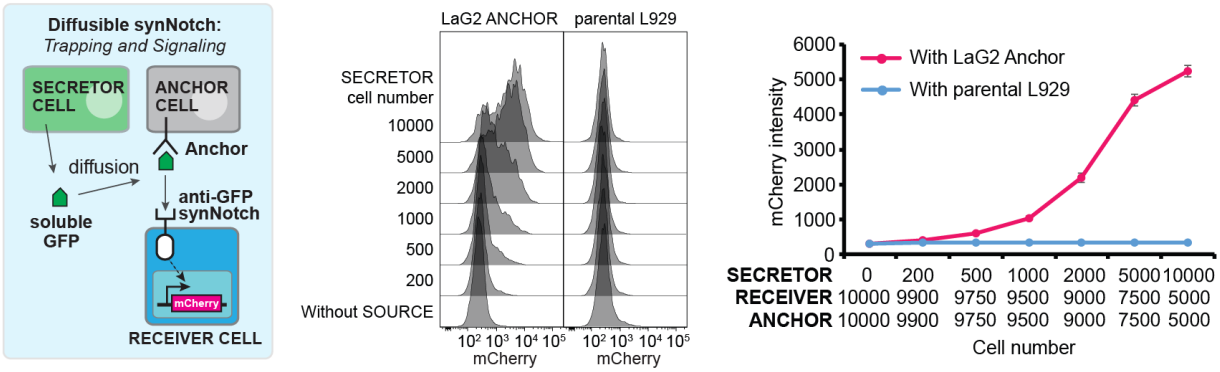

Fig. S1. Testing diffusible GFP synNotch sensing system.

A. Analyzing different GFP nanobodies as Anchor molecules. We engineered L929 cells to express anti-GFP Anchor molecule composed of different GFP nanobody (LaG17, LaG16, LaG9 or LaG2) to test their ability to tether GFP morphogen (*9*). We fused myc-tag to these anti-GFP Anchor molecules and quantified the expression level by staining the cells with anti-myc-Alexa647 antibody. We set up the pole and body regions as shown in Fig.S2A, and plated $3x10^4$ GFP-secreting cells in the pole region and $1.5x10^4$ anti-GFP anchor-expressing cells in the body region. We took images with IN Cell Analyzer 6000 at 24hr when GFP gradient intensity reached maximum. For quantification of GFP distribution, we quantified GFP intensity in the rectangle region by ImageJ with subtraction of GFP intensity on parental L929 as a background to remove the periodic pattern artifact caused by stitching. The relative rank order of GFP intensity with LaG anchors which have the same epitope cite (LaG17, 16, 9) correlates with their reported Kd values, but LaG2 anchor (Kd=16nM) can trap GFP more efficiently than LaG16 anchor (Kd=0.7nM), potentially because our cell culture context is different from the SPR measurements and LaG nanobodies are fused with transmembrane domain which could influence the affinity of nanobodies to GFP.

B. synNotch activation with purified GFP and Anchor cells. We tested three types of receiver cells expressing anti-GFP synNotch (LaG17, LaG16 or LaG9) with LaG2 Anchor cells in the presence of purified GFP (*8*). $1x10^4$ LaG2 anchor-expressing cells and $1x10^4$ anti-GFP synNotch-expressing receiver cells were co-cultured in 96well for 24hr in the presence of indicated amount of purified GFP, followed by analysis with flow cytometry. Without LaG2 Anchor cells, all synNotches showed background activation with a large amount of purified GFP input, but low affinity LaG17 synNotch has the lowest background activity compared to other higher affinity synNotches. Therefore, in our following experiments, we chose a pair of LaG2 anchor and LaG17 synNotch in the diffusible synNotch system, where the LaG2 anchor can tether GFP efficiently and the LaG17 synNotch can interpret the tethered GFP to gene expression output.

C. Dose-dependent synNotch activation by GFP-secreting cells with Anchor cells. We co-cultured GFP-secreting cells, LaG2 anchor-expressing cells and LaG17 synNotch-expressing receiver cells with variations on cell ratio. We fixed the total cell number at $2x10^4$, put the same number of the anchor and receiver cells and changed the number of GFP-secreting cells. This assay was done in triplicate and error bars reflecting standard deviation. The reporter mCherry induction in the receiver cells increased dose-dependently on the number of GFP-secreting cells.

Fig. S2. Characterization of GFP synthetic morphogen gradient formation

A. Experimental setup for in vitro gradient formation.

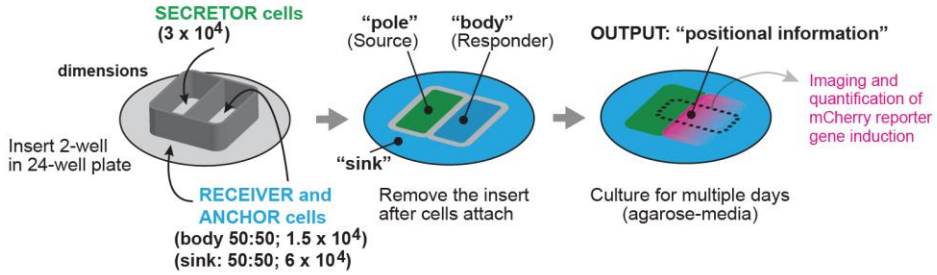

B. Configuration of 3-well poles and body; gradient with 1% agarose media

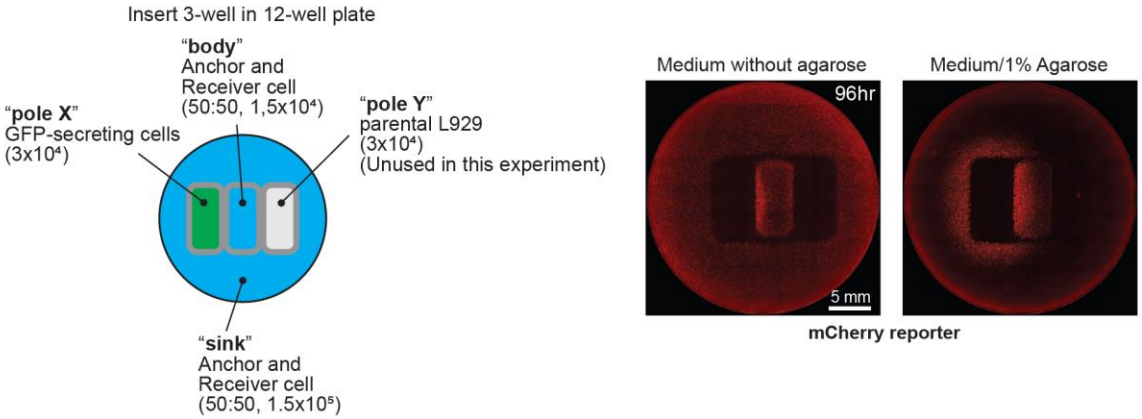

C. Time course and quantification of gradient output (Fig.1D)

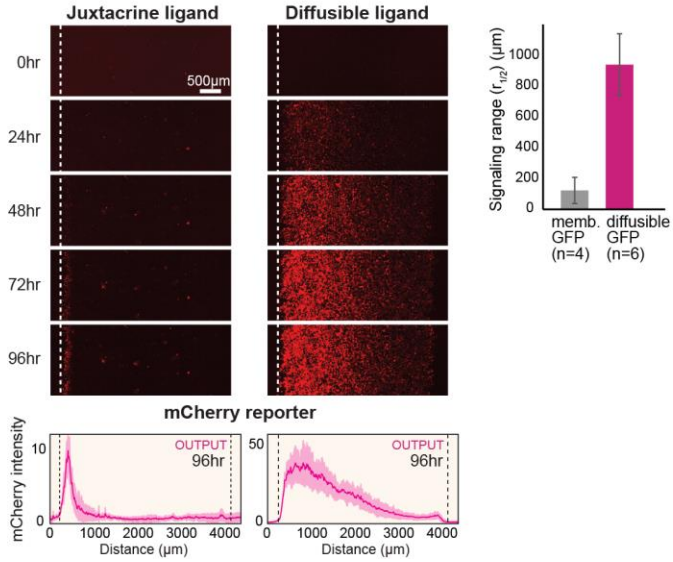

D. Observation of GFP morphogen

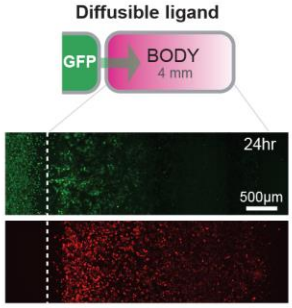

Fig. S2. Characterization of GFP synthetic morphogen gradient formation.

A. Experimental setup for in vitro gradient formation. We put two-well insert wall (ibidi #80209) in 24well and then plated $3x10^4$ GFP-secreting cells in the left "pole" well and $1.5x10^4$ mixture of anchor and receiver cells (50:50) in the right "body" well. We also plated $6x10^4$ mixture of anchor and receiver cell (50:50) in the outside of the insert as a sink. After these cells attached to the plate (5hr incubation in CO2 incubator at 37C), we gently washed the wells and removed the dividing insert. Then we replaced media with 800ul of media containing 1% agarose. Pattern formation was imaged using the incucyte time-lapse microscopy system or IN Cell Analyzer 6000.

B. Gradient formation with 1% agarose media with configuration of 3-well insert wall (two poles and body). We plated $3x10^4$ GFP-secreting cells in the left "pole X", $1.5x10^4$ anchor and receiver mixture cells (50:50) in the middle "body", and $3x10^4$ parental L929 cells in the right "pole Y" (pole Y was not used in this experiment). We also plated $1.5x10^5$ anchor and receiver mixture cells in the outside of the insert-wall as a sink. When we cultured the well without 1% agarose in the media, mCherry induction was spread to the whole well, though gradient was formed in the body to some extent. With 1% agarose media, mCherry induction was restricted in the surrounding of the GFP-secreting pole X. This result suggests that there is a significant random convection flow to spread secreted GFP in normal media.

C. Time course of gradient output (Fig.1D). The images show the time course of mCherry channel in the body region of Fig.1D every 24hr. Juxtacrine signaling by GFPlig started around 48hr because juxtacrine signaling requires direct cell-cell contact and it took around 48hr for cells to fill the gap between the pole and body regions after the insert wall was removed. Diffusible signaling by secreted GFP formed a gradient of mCherry reporter expression and reached steady-state gradient around 96hr. The bottom graphs quantify mCherry reporter expression in the body region at 96hr with error bars (SD) from multiple experiments (Juxtacrine ligand: n=4, Diffusible ligand: n=6). The right graph shows the quantitation of signaling range from multiple experiments ($r_{1/2}$ = distance of half-maximal output).

D. Observation of GFP morphogen. Since GFP channel has high background fluorescence from media with the incucyte system, we observed GFP and mCherry distribution 24hr after plating cells in the same experiment setup of Fig.1D using IN Cell Analyzer 6000. GFP morphogen formed a gradient similarly to Fig.S1A, inducing mCherry reporter gradient.

Fig. S3. Engineering and gradient formation of mCherry-PNE morphogen

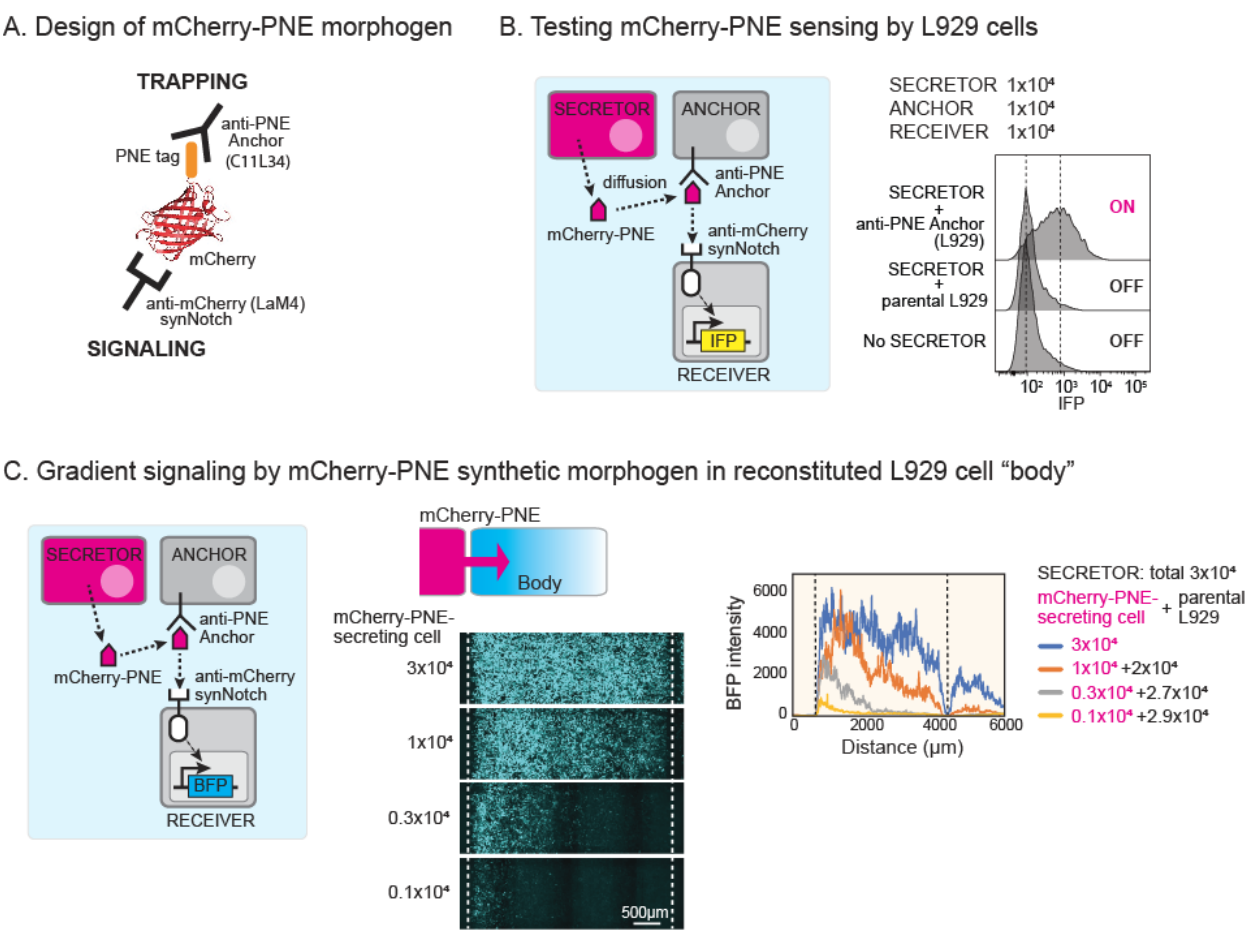

Fig. S3. Engineering and gradient formation of mCherry-PNE morphogen.

A. Design of mCherry-PNE morphogen. mCherry-PNE synthetic morphogen can be tethered by anti-PNE (C11L34) anchor and then activate anti-mCherry (LaM4) synNotch.

B. Testing mCherry-PNE sensing by L929 cells. We co-cultured $1x10^4$ mCherry-PNE-expressing cells, $1x10^4$ anti-PNE anchor-expressing cells and $1x10^4$ anti-mCherry synNotch-expressing receiver cells and analyzed the induction of IFP in the receiver cells with flow cytometry.

C. Gradient signaling by mCherry-PNE synthetic morphogen in reconstituted L929 cell "body". We plated mCherry-PNE-secreting cells in the pole region and $1.5x10^4$ anchor and receiver mixture cells (50:50) in the body region. In this experiment, we fixed a total number of cells at $3x10^4$ in the pole region and changed a ratio of mCherry-PNE-secreting cell and parental L929 as indicated in the figure. We imaged the body region using IN Cell Analyzer at 96hr and quantified the intensity of induced BFP in the rectangle of stitched images with subtraction of background fluorescence measured in blank well. Dose-dependent gradient signaling was observed.

Fig. S4. supplementary studies for anchor density analysis

A. Direct measurement of GFP morphogen gradient (not reporter output) as function of anchor density (parallel to Fig. 2A)

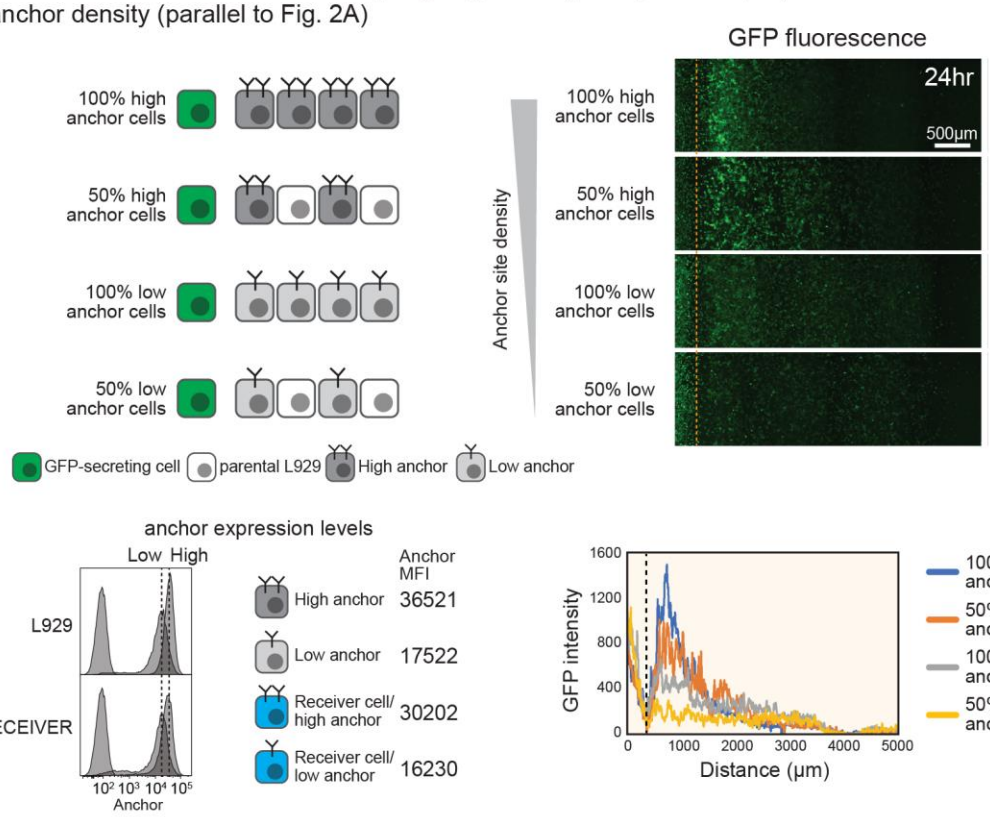

B. Hybrid RECEIVER cells expressing anchor protein show similar response to soluble GFP compared to the co-culture system of separate RECEIVER and Anchor cell (Fig. 2A)

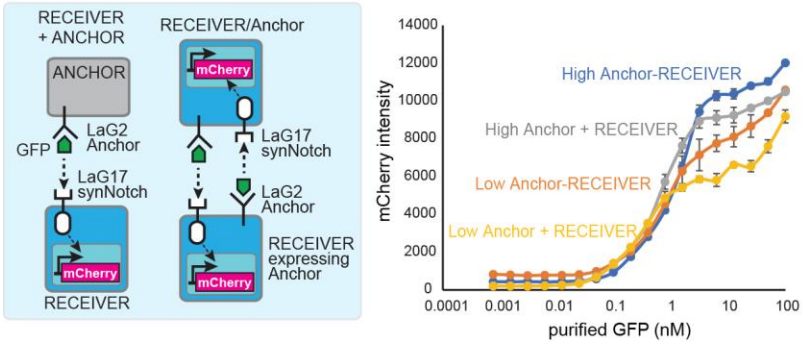

C. Quantification of signaling range of the co-culture system of RECEIVER and HIGH or LOW anchor cell (Fig. 2A)

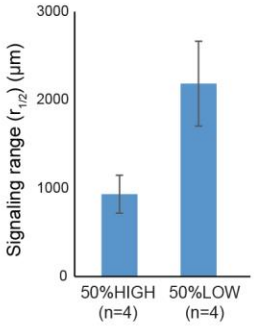

Fig. S4. Supplementary studies for anchor density analysis

A. Direct measurement of GFP morphogen gradient (not reporter output) as function of anchor density (parallel to Fig.2A). $3x10^4$ GFP-secreting cells were plated in the pole region. We plated $1.5x10^4$ anchor cells in the body region with four variations on anchor density: 100% cells express high or low level of anchor; 50% cells express high or low level of anchor. The body region was imaged by IN Cell Analyzer 6000 and quantified the GFP intensity in the rectangle by ImageJ with subtraction of fluorescence on parental L929 as a background. The expression level of LaG2 anchor on L929 cells or synNotch receiver cells was quantified with flow cytometry by staining HA-tag on the LaG2 anchor protein with anit-HA-Alexa647 antibody. The mean fluorescence intensity (MFI) of Alexa647 were indicated.

B. Hybrid RECEIVER cells expressing anchor protein show similar response to soluble GFP compared to the co-culture system of separate RECEIVER and Anchor cell (Fig.2A). We co-cultured $1x10^4$ anchor cells and $1x10^4$ receiver cells or cultured $2x10^4$ hybrid anchor/receiver cells in 96well plate in the presence of indicated amount of purified GFP. After 24hr incubation, mCherry intensity in the receiver cells were measured by flow cytometry. This assay was done in triplicate and error bars show standard deviation. All systems have same sensitivity to soluble GFP, though higher anchor expression can induce more mCherry reporter.

C. Quantification of signaling range of the co-culture system of RECEIVER and HIGH or LOW anchor cell at 96hr (Fig.2A). HIGH anchor cell (50%HIGH) caused shorter signaling range of gradient than LOW anchor cell (50%LOW). The signaling range $r_{1/2}$ was calculated from multiple experiments and error bars show SD.

Fig. S5. Prediction of synthetic morphogen gradient using computational model

A. Prediction of gradient shape from low (GFP system) to high (mCherry-PNE system) anchor affinity

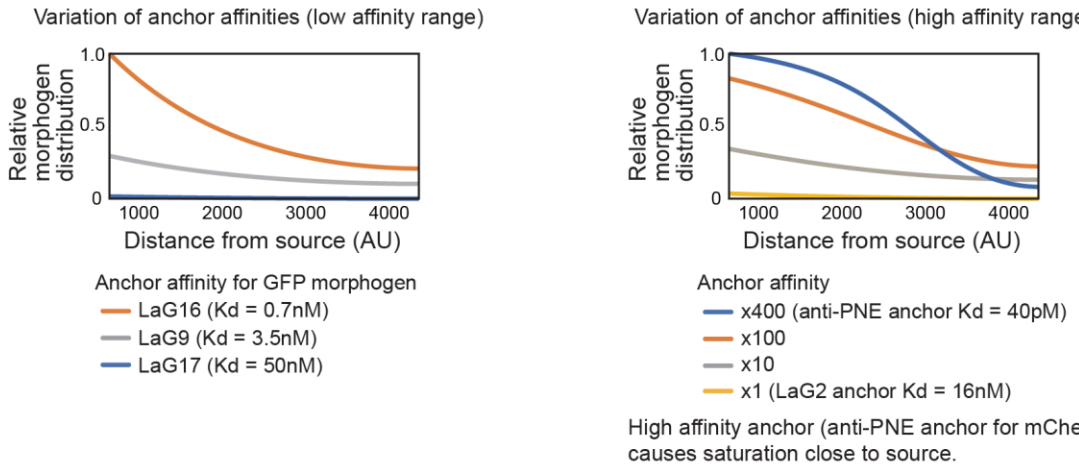

High affinity anchor (anti-PNE anchor for mCherry-PNE) causes saturation close to source.

B. Anchor density defines the steepness of gradient

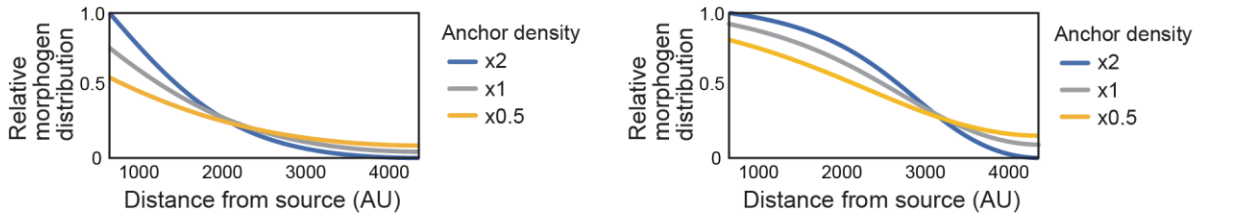

C. Prediction of two types of phenotypes (amplitude and range shift) with Inhibitor pole

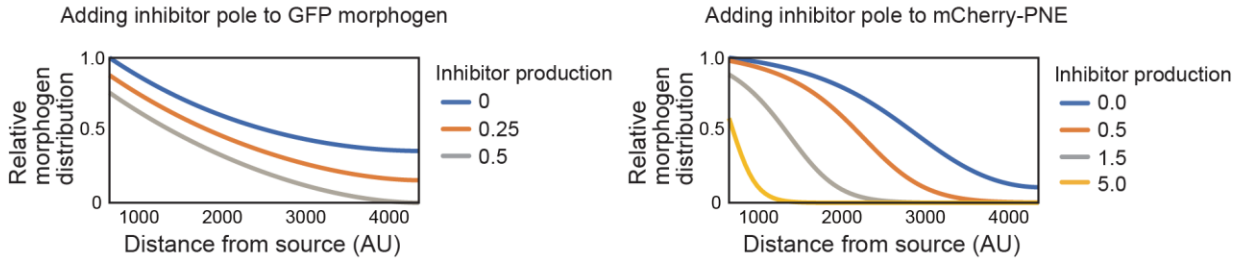

GFP / GFP inhibitor causes amplitude shift

mCherry-PNE / mCherry-PNE inhibitor causes range shift

Fig. S5. Prediction of synthetic morphogen gradient using computational model. (Equations are given in Supplementary Methods.)

A. Prediction of gradient shape from low (GFP system) to high (mCherry-PNE system) anchor affinity. Left: Variation of anchor affinities (low affinity range), using the known dissociation constants K_d for three different GFP nanobodies in epitope group I (LaG17, LaG16, LaG9; see Fig. S1A and (*9*)). The simulation result with LaG variants qualitatively reproduces the observed trends in GFP intensity (Fig.S1A). This leads to a far-from-saturation regime for anchoring and exponential decay -like patterns for relative morphogen distributions. Right: Variation of anchor affinities (high affinity range). In a generalized case with a fixed off-rate (true values unknown), modulating the on-rate from low affinity corresponding to LaG2 anchor to high affinity corresponding to anti-PNE anchor, the anchoring transitions from far-from-saturation to saturation regime. Concomitantly, the relative morphogen distributions transition from exponential decay -like trends to sigmoidal shaped.
B. Anchor density defines the steepness of gradient. Left: Variation of Anchor densities for GFP morphogen. Increasing anchor density in a non-saturating regime gives rise to exponential decay -like patterns with increasing steepness. We tested the arbitrary values (x2, x1, x0.5) of anchor densities in the model because, in Fig.2A, the HIGH anchor cells express LaG2 anchor about twice as much as the LOW anchor cells according to mean fluorescence intensity by antibody staining of anchor in Fig.S4, suggesting that the anchor density ratio (100%HIGH: 100%LOW: 50%HIGH: 50%LOW) is around 2:1:1:0.5. Right: Variation of Anchor densities for mcherry-PNE morphogen. Increasing the anchor density in a saturating regime gives rise to sigmoidal -like patterns with increasing steepness.
C. Prediction of two types of phenotypes (amplitude and range shift) with inhibitor pole. Left: Adding inhibitor pole to GFP morphogen. When anchor proteins are not near saturation with morphogens, the amplitude of gradient is regulated dose-dependently by the inhibitor-secreting cells, qualitatively matching with a trend of Fig.S6C. Right: Adding inhibitor pole to mCherry-PNE. When anchor proteins are close to saturationed with morphogens by increasing the relative anchor and inhibitor affinities corresponding to the known K_d results of anti-PNE anchor and mCherry-PNE inhbitor, the signaling range of gradient was regulated dose-dependently by the inhibitor-secreting cells, which is matched qualitatively matching with a trend of Fig.2B.

Fig. S6. Testing competitive inhibitors for synthetic morphogens

A. Screening of secreted anti-GFP nanobodies for inhibition of synNotch signaling

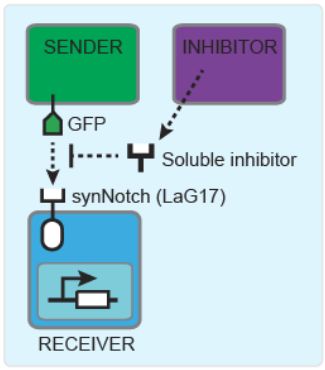

anti-GFP nanobodies Kd
LaG17: 50 nM
LaG16: 0.7 nM
LaG9 : 3.5 nM
LaG2 : 16 nM
LaG16LaG2 : 0.036 nM

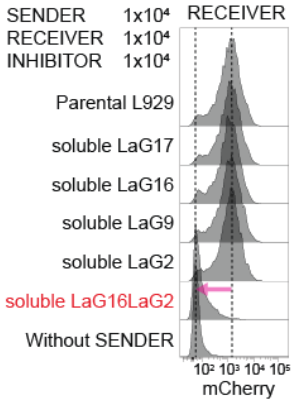

B. Testing mCherry-PNE morphogen inhibitor (used in Fig. 2B)

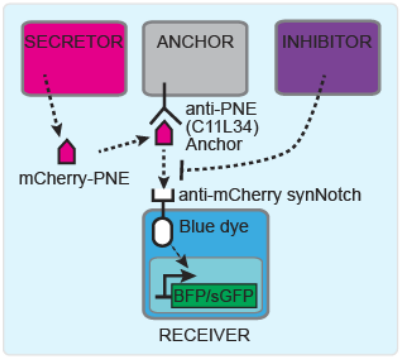

masking inhibitor:
52SR4-LaM4 fusion

anti-PNE scFv Kd
C11L34 : 40pM
52SR4 : 5.2pM

anti-mCherry nanobody Kd
LaM4 : 0.18nM

Coculture in 96-well
5000 SECRETOR
5000 ANCHOR or L929
5000 RECEIVER
5000 INHIBITOR or L929

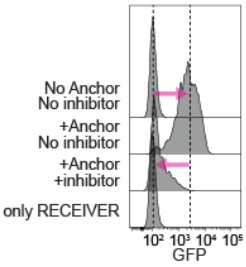

C. Dampening of gradient output by opposing anti-GFP inhibitor pole

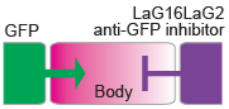

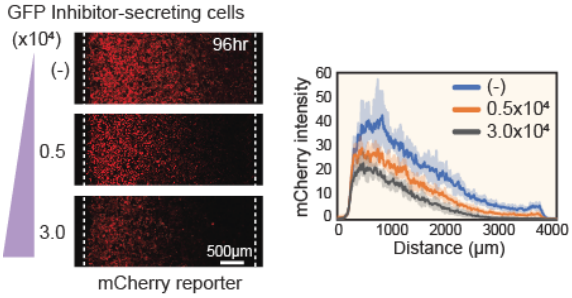

D. Shortening of gradient range by opposing anti-mCherry-PNE inhibitor pole

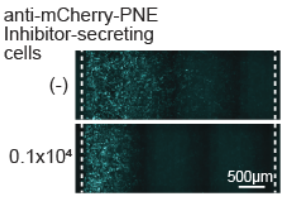

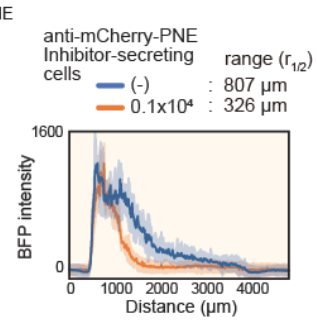

Fig. S6. Testing competitive inhibitors for synthetic morphogens.

A. Screening of secreted anti-GFP nanobodies for inhibition of synNotch signaling. We co-cultured $1x10^4$ GFPlig-expressing cells, $1x10^4$ LaG17 synNotch receiver cells and $1x10^4$ GFP nanobody-secreting cells (LaG17, LaG16, LaG9, LaG2 or LaG16LaG2). The mCherry induction in the receiver cells was quantified by flow cytometry. The list of Kd values of LaG nanobodies is reported in Fridy et al (*9*).

B. Testing mCherry-PNE morphogen inhibitor. According to the result of Fig.S6A, we designed anti-mCherry-PNE-inhibitor by fusing high affinity anti-PNE scFv (52SR4) and anti-mCherry nanobody (LaM4). We co-cultured $5x10^3$ mCherry-PNE-expressing cells, $5x10^3$ anti-PNE anchor-expressing cells, $5x10^3$ anti-mCherry synNotch receiver cells and $5x10^3$ anti-mCherry-PNE-inhibitor-expressing cells and quantified GFP induction in the receiver cells by flow cytometry. The list of Kd values of anti-PNE scFvs and LaM4 nanobody is reported in Fridy et al (*9*) and Zahnd et al (*23*).

C. Dampening of gradient output by opposing anti-GFP inhibitor pole. We plated $3x10^4$ GFP-secreting cells in the left pole. $1.5x10^4$ anchor and receiver mixture cells (50:50) were plated in the middle body. We also plated $1.5x10^5$ anchor and receiver mixture cells (50:50) in the outside of the insert well as a sink. For the inhibitor-secreting right pole, we tested three variations on the number of anti-GFP inhibitor-expressing cells as indicated. The amplitude of GFP gradient signaling can be controlled by anti-GFP inhibitor in a dose-dependent manner. The plate was imaged by incucyte. The mCherry intensity in the rectangle area was quantified with ImageJ. The shaded area shows SD from three experiments.

D. Shortening of gradient signaling range by opposing anti-mCherry-PNE pole. We plated $0.3x10^4$ mCherry-PNE-secreting cells with $2.7x10^4$ parental L929 cells (total $3x10^4$ cells) in the left pole. $1.5x10^4$ mixture of anti-PNE anchor cells and anti-mCherry receiver cells (50:50) were plated in the middle body. We also plated $1.5x10^5$ the anchor and receiver mixture cells (50:50) in the outside of the insert well as a sink. For the inhibitor-secreting right pole, we plated $0.1x10^4$ inhibitor-secreting cells with $2.9x10^4$ parental L929 cells (total $3x10^4$ cells). The signaling range of mCherry-PNE gradient can be reduced with no change on amplitude of activation gradient. The plate was imaged by InCell Analyzer 6000 and the BFP expression was quantified with ImageJ. The shaded area shows SD from triplicates.

Fig. S7. Establishment of positive and negative feedback cell lines (from Fig. 3)

A. Testing GFP morphogen positive feedback cells (L929: anti-GFP synNotch --> GFP))

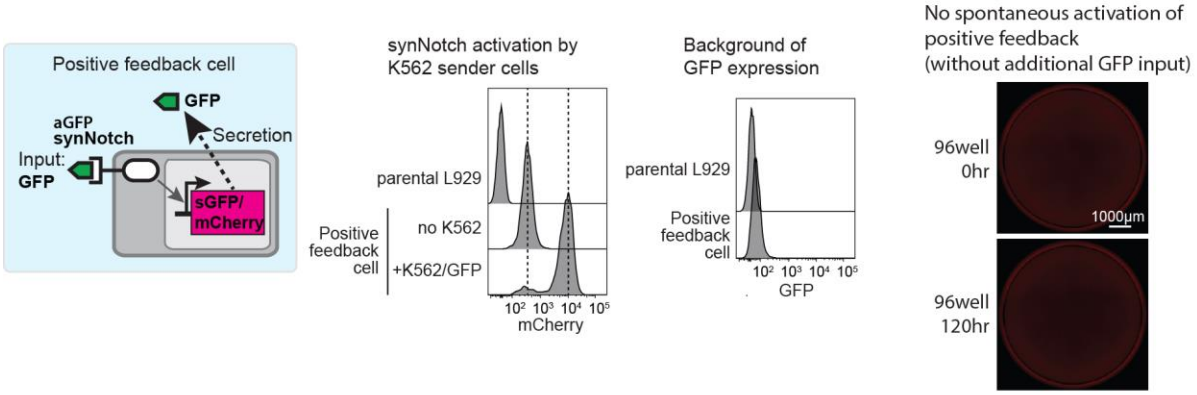

B. Testing GFP morphogen negative feedback cells (L929: anti-GFP synNotch --> anti-GFP inihibitor)

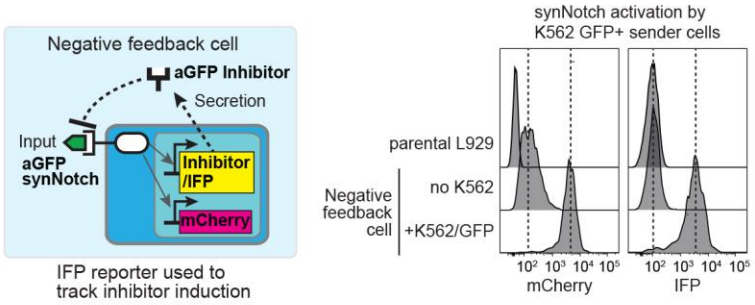

C. Time evolution of signal propagation with positive feedback

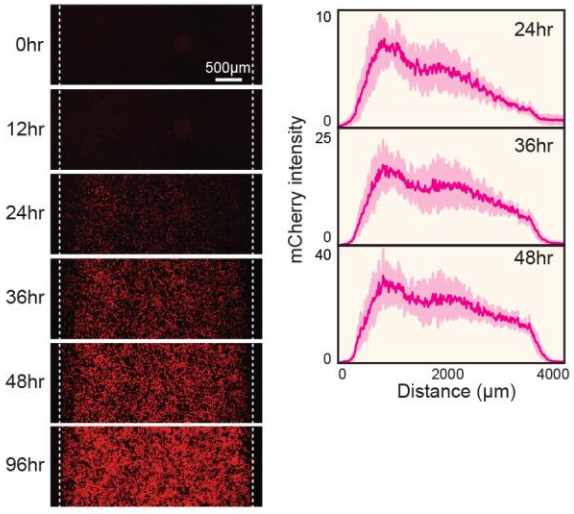

D. Time course of mCherry output by negative feedback (Fig.3D)

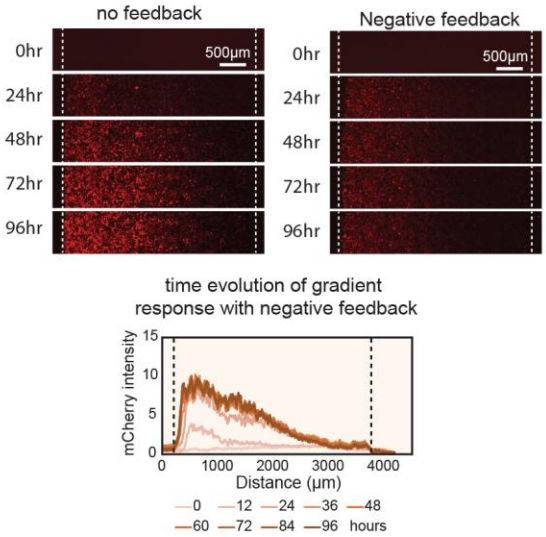

Fig. S7. Establishment of positive and negative feedback cell lines (from Fig. 3).

A. Testing GFP morphogen positive feedback cells (L929: anti-GFP synNotch --> GFP)). We engineered L929 cells to express anti-GFP LaG17 synNotch that induces soluble GFP and mCherry reporter. The expression level of mCherry was measured with or without synNotch stimulation by GFPlig-expressing K562 cells by flow cytometry. We also checked that basal GFP expression level of the positive feedback cell is very low. We co-cultured $1.5x10^4$ positive feedback cells and anchor cells (50:50) for 120hr in 96well and confirmed spontaneous activation of positive feedback circuit did not occur.
B. Testing GFP morphogen negative feedback cells (L929: anti-GFP synNotch --> anti-GFP inhibitor). We engineered L929 cells to express anti-GFP LaG17 synNotch that induces mCherry reporter, soluble anti-GFP inhibitor LaG16LaG2 with NLS-IFP. The expression level of mCherry and IFP were measured with or without synNotch stimulation by GFPlig-expressing K562 cells by flow cytometry.
C. Time course images of signal activation by positive feedback circuit. We plated $3x10^4$ GFP-secreting cells in the pole and $1.5x10^4$ mixture of anchor cells and receiver cells engineered with positive feedback circuit (50:50) in the body region. We also plated $6x10^4$ mixture of LaG2 anchor cells and receiver cells lacking feedback (50:50) in the outside of the insert well as a sink. The plate was imaged by incucyte system for 4 days. The fluorescence profile of mCherry reporter expression in body shows signal propagation from gradient shape at 24hr to whole activation of body at 48hr. The shaded area shows SD from four experiments.
D. Time course images of gradient formation by negative feedback circuit. We plated $3x10^4$ GFP-secreting cells in the pole and $1.5x10^4$ mixture of LaG2 anchor cells and receiver cells engineered with negative feedback circuit (50:50) in the body region. We also plated $6x10^4$ mixture of anchor cells and receiver cells lacking feedback (50:50) in the outside of the insert well as a sink. The plate was imaged by incucyte system for 4 days. While the fluorescence intensity of receiver cells with no feedback gradient gradually increased, the receiver cells with negative feedback formed a low-intensity but steady-state gradient quickly (around 24hr). The time course of mCherry output in the body region was quantified every 12hr.

Fig. S8. Supplemental data on engineering higher-order multi-stripe patterning circuits (Fig. 4)

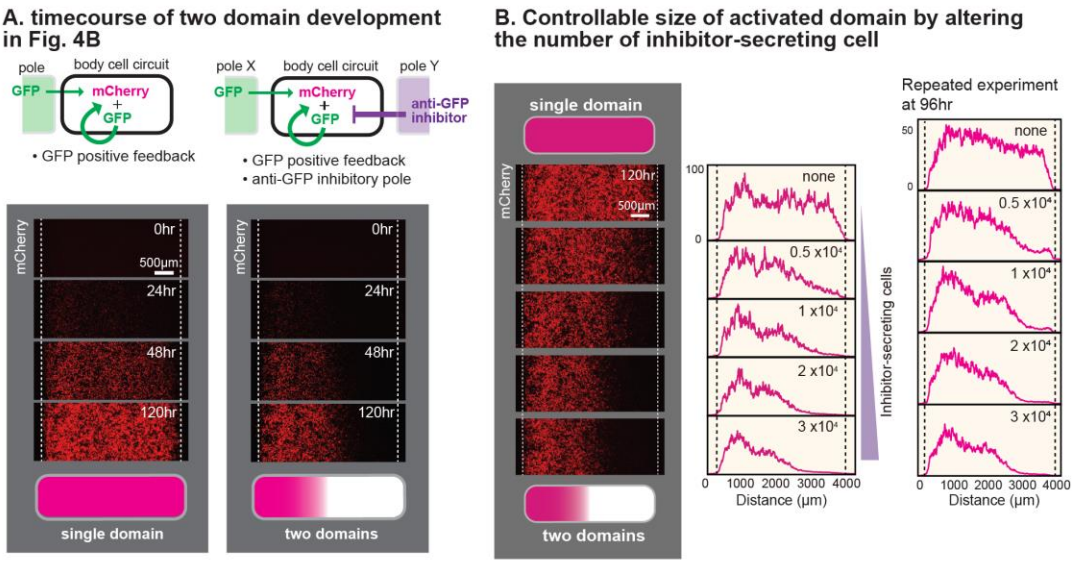

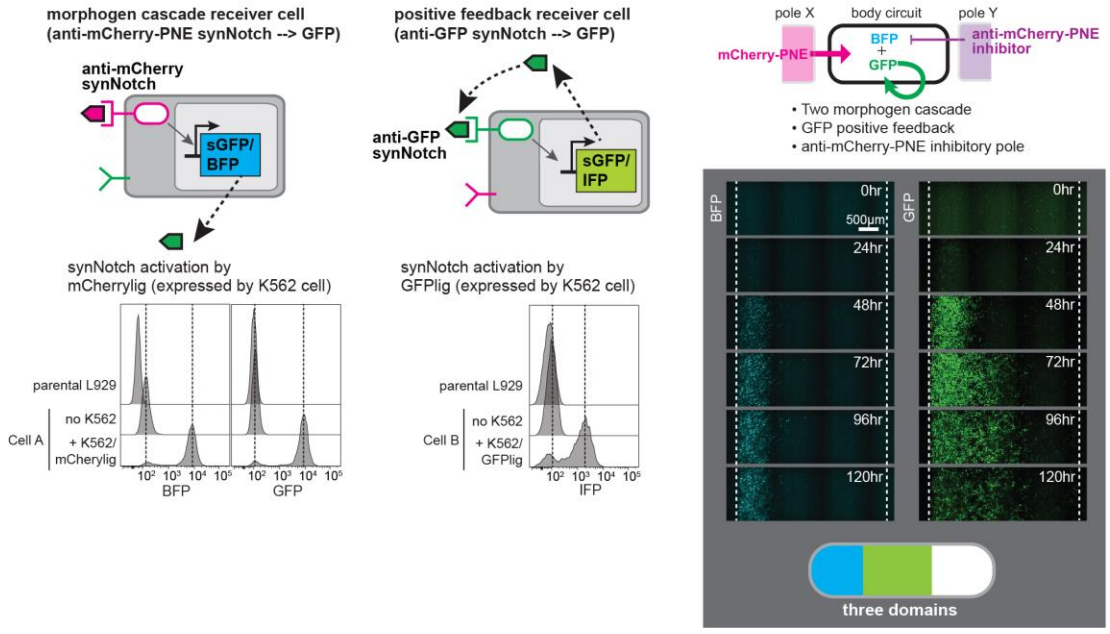

Fig. S8 Supplemental data on engineering higher-order multi-stripe patterning circuits (Fig. 4)

A. Time course of two-domain development in Fig.4B. The images show the time course of mCherry channel in the body region of Fig.4B with or without inhibitor-secreting pole. The positive feedback circuit induced signal activation in the whole body, but when inhibitor cells (mixture of $2x10^4$ anti-GFP inhibitor cells and $1x10^4$ parental L929) were plated in the right pole, signal amplification by positive feedback occurred only at the left half of the body region, leading to forming activated and inactivated domains.
B. Controllable size of activated domain by altering the number of inhibitor-secreting cell. Morphogen pole has $3x10^4$ GFP-secreting cells; Body has 50:50 mixture of anchor cells and receiver cells with positive feedback (used in Fig.3B) ($1.5x10^4$ total cells); inhibitor pole (Y) has variable numbers of anti-GFP inhibitor-secreting cells. The images were taken by incucyte at 120hr. Plots indicate the number of inhibitor-secreting cells plated within pole Y (out of $3x10^4$ total cells). The right plots show the data at 96hr from a repeated experiment with same experimental setup, showing the reproducibility of two-domain patterning.
C. Testing receiver cells used in three stripe pattern (Fig.4C,D). For morphogen cascade receiver cell, we engineered L929 cells to express anti-mCherry synNotch that induces soluble GFP and BFP reporter. The expression level of BFP and GFP was measured with or without synNotch stimulation by mCherrylig-expressing K562 cells by flow cytometry. The morphogen cascade receiver cell was also engineered to express anti-GFP LaG2 anchor. For positive feedback receiver cell, we engineered L929 cells to express anti-GFP LaG17 synNotch that induces soluble GFP and NLS-IFP reporter. The expression level of IFP was measured with or without synNotch stimulation by GFPlig-expressing K562 cells by flow cytometry. The positive feedback receiver cell was also engineered to express anti-PNE anchor.
D. Time course of three-domain development in Fig.4D. The images show time course of BFP and GFP channels in the body region of Fig.4D every 24hr. Around 48hr, mCherry-PNE and anti-mCherry-PNE inhibitor poles generated the narrow BFP^+GFP^+ domain as shown in Fig.2B. Then induced GFP activated the positive feedback of GFP morphogen, which generated BFP^-GFP^+ domain at 72hr. As the amount of GFP from narrow BFP^+GFP^+ domain was not enough to induce propagation of GFP morphogen to the end of the body, BFP^-GFP^- domain close to the inhibitor pole was maintained at 96hr or later.

Fig. S9. Engineering bottom up positional information with anchoring and signaling of secreted protein

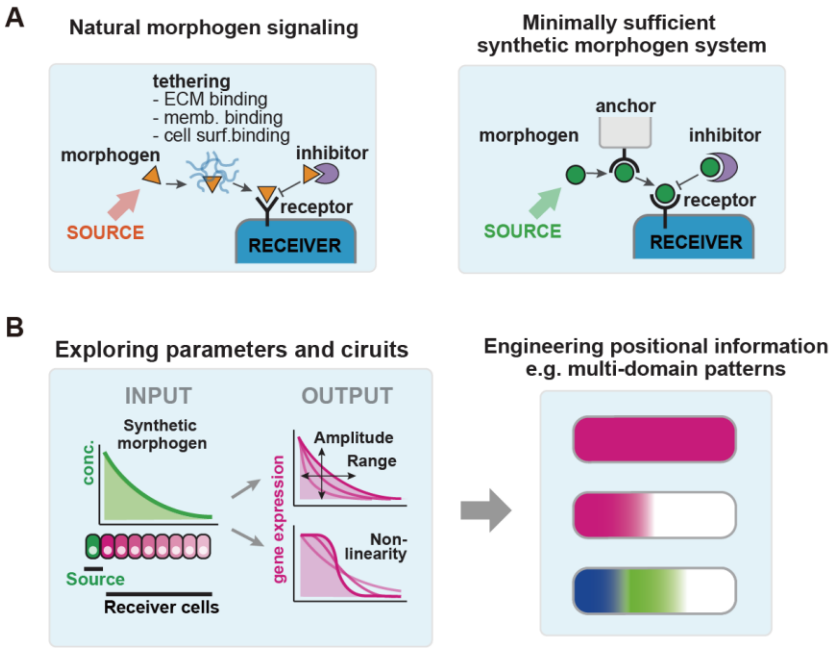

Fig. S9. Engineering bottom up positional information with anchoring and signaling of secreted protein

(A) Differences and commonalities between synthetic and natural morphogen systems. While our synthetic morphogens require an explicit anchoring protein, many natural morphogens have diverse interactions that play a tethering function (e.g. interactions with ECM, cell surface proteins, and direct membrane interactions). There are likely many alternative tethering solutions that constrain morphogen diffusion and control gradient shape.

(B) Synthetic morphogen systems allow exploration of patterning circuit design space, as well as forward engineering of de novo patterns.

Fig. S10. Engineering lipidated synthetic morphogen composed of Sonic hedgehog (Shh) fusion with GFP

A. Construction of Shh-GFP

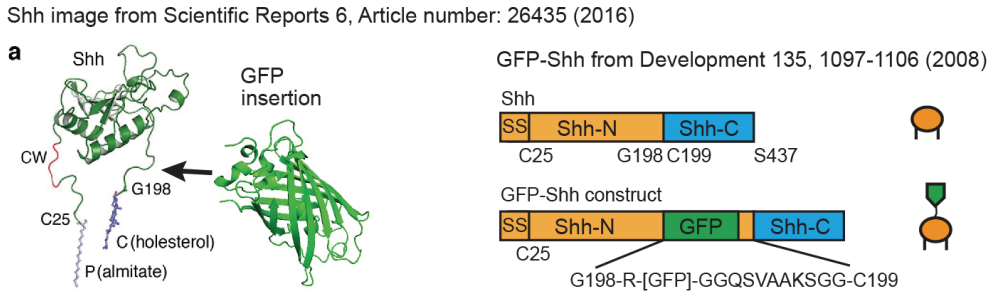

B. Testing anti-GFP synNotch signaling by Shh-GFP fusion

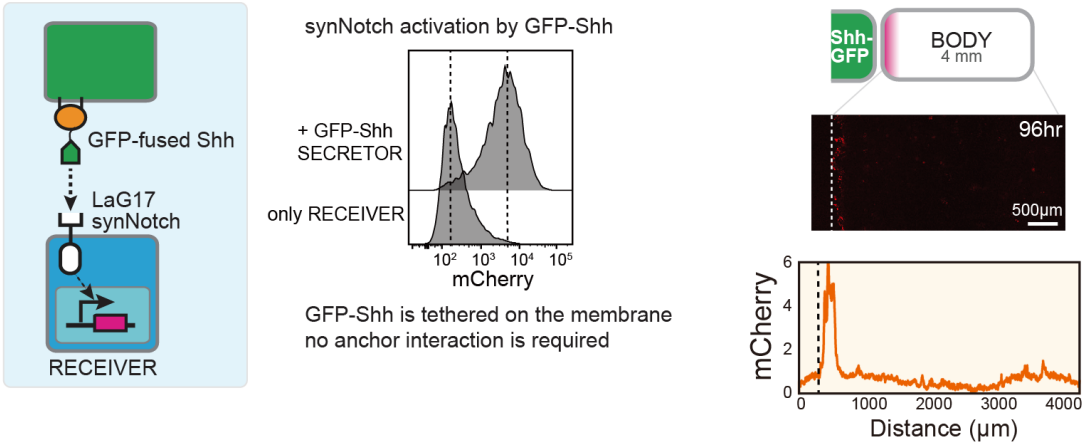

Fig. S10 Engineering lipidated synthetic morphogen composed of Sonic hedgehog (Shh) fusion with GFP

A. Construction of Shh-GFP. Image was reproduced from (*27*). Shh-GFP was developed in (*20*). GFP was inserted between Shh protein and C-terminal cholesterol modification.
B. Testing anti-GFP synNotch signaling by Shh-GFP fusion. We co-cultured $1x10^4$ Shh-GFP-expressing cells and $1x10^4$ LaG17 synNotch-expressing receiver cells in 96well for 24hrs. mCherry intensity in the receiver cells were quantified by flow cytometry. For the gradient assay using Shh-GFP, we plated $3x10^4$ Shh-GFP-expressing cells in the pole and $1.5x10^4$ LaG17 synNotch receiver cells in the body. The mCherry reporter gene expression was only observed at the boundary between the pole and body. Image was taken by incucyte at 96hr. The mCherry intensity in the rectangle area at 96hr was quantified.

Fig. S11. Engineering diffusible synNotch system in primary human T cell

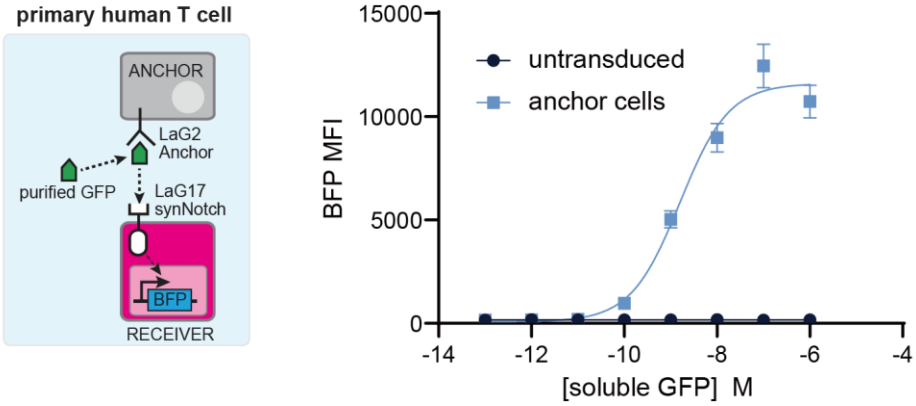

Fig. S11. Engineering diffusible synNotch system in primary human T cell

Primary Human T cells were engineered to express LaG2 anchor as an anchor cell and express LaG17 synNotch that induces BFP reporter as a receiver cell. $5x10^4$ cells of anchor and receiver cells were cocultured for 24hrs in the presence of indicated amounts of purified GFP, followed by analysis with flow cytometry. In addition to L929 fibroblasts, the diffusible synNotch system with anchor and receiver cell functioned in primary human T cells.

Table 1. Summary of experimental conditions of gradient assay in each figure.

Figures	plate	ibidi insert	morphogen pole	body	inhibitory pole	sink
Fig. 1D, Fig. S2C	12well	3well	3x10^4 cells expressing membrane GFP	1.5x10^4 Receiver	3x10^4 L929 (unused)	1.5x10^5 Receiver
Fig. 1D, Fig. S2B-D, MovieS1	12well	3well	3x10^4 GFP-secreting cells	1.5x10^4 Receiver + Anchor	3x10^4 L929 (unused)	1.5x10^5 Receiver + Anchor
Fig. 2A	24well	2well	3x10^4 GFP-secreting cells	1.5x10^4 Receiver + HIGH or LOW Anchor 1.5x10^4 HIGH or LOW hybrid Receiver/Anchor	no pole	6x10^4 same cells in the body
Fig. 2B	12well	3well	1x10^4 mCherryPNE-secreting cells + 2x10^4 L929	1.5x10^4 Receiver + Anchor	1x10^4 Inhibitor + 2x10^4 L929 0.3x10^4 Inhibitor + 2.7x10^4 L929 0.1x10^4 Inhibitor + 2.9x10^4 L929 3x10^4 L929	1.5x10^5 Anchor + L929
Fig. 3B-C, Fig. S7C, Movie S1	12well	3well	3x10^4 GFP-secreting cells	1.5x10^4 Positive feedback Receiver + Anchor	3x10^4 L929 (unused)	1.5x10^5 Receiver + Anchor
Fig. 3D, Fig. S7D	12well	2well	3x10^4 GFP-secreting cells	1.5x10^4 Negative feedback Receiver + Anchor	no pole	1.5x10^5 Receiver + Anchor
Fig. 4B, Fig. S8A-B, MovieS1	12well	3well	3x10^4 GFP-secreting cells	1.5x10^4 Positive feedback Receiver + Anchor	3x10^4 Inhibitor 2x10^4 Inhibitor + 1x10^4 L929 1x10^4 Inhibitor + 2x10^4 L929 0.5x10^4 Inhibitor + 2.5x10^4 L929 3x10^4 L929	1.5x10^5 Receiver + Anchor
Fig. 4D, Fig. S8D	12well	3well	0.3x10^4 mCherryPNE-secreting cells + 2.7x10^4 L929	1.5x10^4 Receiver A + Receiver B	0.1x10^4 mCherry-PNE Inhibitor + 2.9x10^4 L929	1.5x10^5 mCherry-PNE Anchor + L929
Fig. S1A	24well	2well	3x10^4 GFP-secreting cells	1.5x10^4 Anchor cells with variable LaGs	no pole	6x10^4 same cells in the body
Fig. S3C	24well	2well	0.1x10^4 mCherryPNE-secreting cells + 2.9x10^4 L929 0.3x10^4 mCherryPNE-secreting cells + 2.7x10^4 L929 1x10^4 mCherryPNE-secreting cells + 2x10^4 L929 3x10^4 mCherryPNE-secreting cells	1.5x10^4 Receiver + Anchor	no pole	6x10^4 Receiver + Anchor
Fig. S4A	24well	2well	3x10^4 GFP-secreting cells	1.5x10^4 HIGH or LOW Anchor + L929 1.5x10^4 HIGH or LOW Anchor	no pole	6x10^4 same cells in the body
Fig. S4C	24well	2well	3x10^4 GFP-secreting cells	1.5x10^4 Receiver + HIGH or LOW Anchor	no pole	6x10^4 same cells in the body
Fig. S6C	12well	3well	3x10^4 GFP-secreting cells	1.5x10^4 Receiver + Anchor	3x10^4 Inhibitor 0.5x10^4 Inhibitor + 2.5x10^4 L929 3x10^4 L929	1.5x10^5 Receiver + Anchor
Fig.S6D	12well	3well	0.3x10^4 mCherryPNE-secreting cells + 2.7x10^4 L929	1.5x10^4 Receiver + Anchor	0.1x10^4 mCherry-PNE Inhibitor + 2.9x10^4 L929 3x10^4 L929	1.5x10^5 mCherry-PNE Anchor + L929
Fig. S10B	12well	3well	3x10^4 Shh-GFP-secreting cells	1.5x10^4 Receiver	3x10^4 L929 (unused)	1.5x10^5 Receiver
Movie S2	12well	3well	0.6x10^4 mCherryPNE-secreting cells + 2.4x10^4 L929	1.5x10^4 Receiver + Anchor	0.6x10^4 mCherry-PNE Inhibitor + 2.4x10^4 L929	1.5x10^5 mCherry-PNE Anchor + L929

Table 1. Summary of experimental conditions of gradient assay in each figure.

Movie S1. Altering shape of gradient response linked to Fig.1, Fig.3 and Fig.4.

Time-lapse movie showing both dynamics and altering interpretation of gradient signaling by engineered cell-cell circuits in Fig.1D, Fig.S2, Fig.3B, Fig.4B and Fig.S8A-B. This movie was taken by IncuCyte with 4x objective at 2hrs/frame for 96hr and 120hr, respectively. In response to gradient signal of synthetic morphogen GFP from the pole region, positive feedback circuits induced signal propagation and formed single domain of active cells in the body region (left). On the other hand, putting opposing inhibitor-secreting pole, two activated and inactivated domains were formed with non-linear transition (right).

Movie S2. Formation of three distinct domains linked to Fig.4.

Time-lapse movie showing the dynamics of three domain formation in Fig.4D and Fig.S8D. This movie was taken by Opera Phenix with 10x objective at 2hrs/frame for 72hr. mCherry-PNE morphogen formed narrow $BFP^{+}GFP^{+}$ domain first, and then GFP morphogen activated positive feedback circuit to induce limited propagation of GFP^{+} domain, leading to the formation of $BFP^{-}GFP^{+}$ and $BFP^{-}GFP^{-}$ domain.

References and Notes

1. A. M. Turing, The Chemical Basis of Morphogenesis. *Phil. Trans. R. Soc. Lond. B* **237**, 37–72 (1952). doi:10.1098/rstb.1952.0012

2. L. Wolpert, Positional information and the spatial pattern of cellular differentiation. *J. Theor. Biol.* **25**, 1–47 (1969). doi:10.1016/S0022-5193(69)80016-0 Medline

3. K. W. Rogers, A. F. Schier, Morphogen gradients: From generation to interpretation. *Annu. Rev. Cell Dev. Biol.* **27**, 377–407 (2011). doi:10.1146/annurev-cellbio-092910-154148 Medline

4. A. D. Lander, How cells know where they are. *Science* **339**, 923–927 (2013). doi:10.1126/science.1224186 Medline

5. T. Tabata, Y. Takei, Morphogens, their identification and regulation. *Development* **131**, 703–712 (2004). doi:10.1242/dev.01043 Medline

6. P. Li, J. S. Markson, S. Wang, S. Chen, V. Vachharajani, M. B. Elowitz, Morphogen gradient reconstitution reveals Hedgehog pathway design principles. *Science* **360**, 543–548 (2018). doi:10.1126/science.aao0645 Medline

7. R. Sekine, T. Shibata, M. Ebisuya, Synthetic mammalian pattern formation driven by differential diffusivity of Nodal and Lefty. *Nat. Commun.* **9**, 5456 (2018). doi:10.1038/s41467-018-07847-x Medline

8. L. Morsut, K. T. Roybal, X. Xiong, R. M. Gordley, S. M. Coyle, M. Thomson, W. A. Lim, Engineering Customized Cell Sensing and Response Behaviors Using Synthetic Notch Receptors. *Cell* **164**, 780–791 (2016). doi:10.1016/j.cell.2016.01.012 Medline

9. P. C. Fridy, Y. Li, S. Keegan, M. K. Thompson, I. Nudelman, J. F. Scheid, M. Oeffinger, M. C. Nussenzweig, D. Fenyö, B. T. Chait, M. P. Rout, A robust pipeline for rapid production of versatile nanobody repertoires. *Nat. Methods* **11**, 1253–1260 (2014). doi:10.1038/nmeth.3170 Medline

10. E. M. De Robertis, H. Kuroda, Dorsal-ventral patterning and neural induction in Xenopus embryos. *Annu. Rev. Cell Dev. Biol.* **20**, 285–308 (2004). doi:10.1146/annurev.cellbio.20.011403.154124 Medline

11. E. Bier, E. M. De Robertis, BMP gradients: A paradigm for morphogen-mediated developmental patterning. *Science* **348**, aaa5838 (2015). doi:10.1126/science.aaa5838 Medline

12. A. Eldar, D. Rosin, B.-Z. Shilo, N. Barkai, Self-enhanced ligand degradation underlies robustness of morphogen gradients. *Dev. Cell* **5**, 635–646 (2003). doi:10.1016/S1534-5807(03)00292-2 Medline

13. D. Yan, X. Lin, Shaping morphogen gradients by proteoglycans. *Cold Spring Harb. Perspect. Biol.* **1**, a002493 (2009). doi:10.1101/cshperspect.a002493 Medline

14. A. Parchure, N. Vyas, S. Mayor, Wnt and Hedgehog: Secretion of Lipid-Modified Morphogens. *Trends Cell Biol.* **28**, 157–170 (2018). doi:10.1016/j.tcb.2017.10.003 Medline

15. Y. Wang, X. Wang, T. Wohland, K. Sampath, Extracellular interactions and ligand degradation shape the nodal morphogen gradient. *eLife* **5**, e13879 (2016). doi:10.7554/eLife.13879 Medline

16. P. Müller, K. W. Rogers, S. R. Yu, M. Brand, A. F. Schier, Morphogen transport. *Development* **140**, 1621–1638 (2013). doi:10.1242/dev.083519 Medline

17. T. B. Kornberg, A. Guha, Understanding morphogen gradients: A problem of dispersion and containment. *Curr. Opin. Genet. Dev.* **17**, 264–271 (2007). doi:10.1016/j.gde.2007.05.010 Medline

18. K. S. Stapornwongkul, M. de Gennes, L. Cocconi, G. Salbreux, J.-P. Vincent, Patterning and growth control in vivo by an engineered GFP gradient. *Science* **370**, 321–327 (2020). doi:10.1126/science.abb8205

19. B. Stern, L. C. Olsen, C. Trösse, H. Ravneberg, I. F. Pryme, Improving mammalian cell factories: The selection of signal peptide has a major impact on recombinant protein synthesis and secretion in mammalian cells. *Trends Cell Mol. Biol.* **2**, 1–17 (2007); www.unitargeting.com/Resources/Trends07.pdf.

20. C. E. Chamberlain, J. Jeong, C. Guo, B. L. Allen, A. P. McMahon, Notochord-derived Shh concentrates in close association with the apically positioned basal body in neural target cells and forms a dynamic gradient during neural patterning. *Development* **135**, 1097–1106 (2008). doi:10.1242/dev.013086 Medline

21. J. Hanes, L. Jermutus, S. Weber-Bornhauser, H. R. Bosshard, A. Plückthun, Ribosome display efficiently selects and evolves high-affinity antibodies in vitro from immune libraries. *Proc. Natl. Acad. Sci. U.S.A.* **95**, 14130–14135 (1998). doi:10.1073/pnas.95.24.14130 Medline

22. D. Yu, W. C. Gustafson, C. Han, C. Lafaye, M. Noirclerc-Savoye, W.-P. Ge, D. A. Thayer, H. Huang, T. B. Kornberg, A. Royant, L. Y. Jan, Y. N. Jan, W. A. Weiss, X. Shu, An improved monomeric infrared fluorescent protein for neuronal and tumour brain imaging. *Nat. Commun.* **5**, 3626 (2014). doi:10.1038/ncomms4626 Medline

23. C. Zahnd, S. Spinelli, B. Luginbühl, P. Amstutz, C. Cambillau, A. Plückthun, Directed in vitro evolution and crystallographic analysis of a peptide-binding single chain antibody fragment (scFv) with low picomolar affinity. *J. Biol. Chem.* **279**, 18870–18877 (2004). doi:10.1074/jbc.M309169200 Medline

24. N. Balaskas, A. Ribeiro, J. Panovska, E. Dessaud, N. Sasai, K. M. Page, J. Briscoe, V. Ribes, Gene regulatory logic for reading the Sonic Hedgehog signaling gradient in the vertebrate neural tube. *Cell* **148**, 273–284 (2012). doi:10.1016/j.cell.2011.10.047 Medline

25. J. Cotterell, J. Sharpe, An atlas of gene regulatory networks reveals multiple three-gene mechanisms for interpreting morphogen gradients. *Mol. Syst. Biol.* **6**, 425 (2010). doi:10.1038/msb.2010.74 Medline

26. B. Z. Shilo, N. Barkai, Buffering Global Variability of Morphogen Gradients. *Dev. Cell* **40**, 429–438 (2017). doi:10.1016/j.devcel.2016.12.012 Medline

27. P. Jakobs, P. Schulz, C. Ortmann, S. Schürmann, S. Exner, R. Rebollido-Rios, R. Dreier, D. G. Seidler, K. Grobe, Bridging the gap: Heparan sulfate and Scube2 assemble Sonic hedgehog release complexes at the surface of producing cells. *Sci. Rep.* **6**, 26435 (2016). doi:10.1038/srep26435 Medline